IEEE Access
Multidisciplinary ⋮ Rapid Review ⋮ Open Access Journal

Received December 30, 2019, accepted January 9, 2020, date of publication January 13, 2020, date of current version January 23, 2020.

Digital Object Identifier 10.1109/ACCESS.2020.2966225

Omnidirectional and Efficient Wireless Power Transfer System for Logistic Robots

ZHENG ZHANG AND BO ZHANG, (Senior Member, IEEE)
School of Electric Power, South China University of Technology, Guangzhou 510641, China

Corresponding author: Bo Zhang (epbzhang@scut.edu.cn)

This work was supported by the Key Program of National Natural Science Foundation of China under Grant 51437005.

ABSTRACT The WPT system for logistic robots has the problems of large fluctuation of charging power and low efficiency due to the change of its position. Based on the principle of parity time symmetry, an omnidirectional and efficient wireless power transfer system for logistic robots is proposed. Firstly, the coupling coefficient of two planar spiral coils in different relative positions in space are studied. Then, a time-varying coupled-mode model of the WPT system based on the offset angle of the receiver coil is established, and its working principle and characteristics are analyzed. As long as the coupling coefficient satisfies certain conditions, the output power and efficiency of the system are always keeping constant. Finally, the proposed model is experimentally verified. The measured results show that the WPT system proposed can realize stable 150W power transfer with constant transmitting efficiency of more than 90% for a logistic robot within a confined three-dimensional space around the charging station, which are provided to further verify the correctness of theoretical analysis.

INDEX TERMS Wireless power transfer, omnidirectional, parity time symmetry, coupled-mode theory, logistic robots.

I. INTRODUCTION

In recent years, due to its high degree of automation and strong adaptability, logistic robots play an increasingly important role in automation and intelligent industrial production activities, and widely used in automotive, electronics, e-commerce and other fields [1]–[3]. At present, logistic robots are mainly charged by cable, it has the disadvantages of large battery consumption, short cruising range and long charging time [4], and the use of cable charging greatly limits the charging position of the logistics robot, which has been unable to meet the characteristics of the fully automated operation of the logistics robot. A new charging mode is needed to solve this problem. With the continuous exploration of scholars, the wireless power transfer technology has been greatly developed and matured [5]–[7]. If we can build a batch of distributed wireless charging stations in the factory [8], when the logistic robots need to be recharged, it can actively find the nearest charging station for quick replenishment and then be able to re-enter the work in the shortest time. This will completely change the existing working mode of logistic robots and greatly improve the automation and intelligence level of the factory.

However, in a conventional magnetic field coupled wireless power transfer system, only when the transmitter and receiver coils are coaxially aligned, the efficiency of the system can be maximized [9]. Moreover, the existing WPT system often causes the output power to fluctuate drastically due to the change of the load position, and the energy transmitting efficiency is drastically reduced. In the actual application scenario, the relative positions of the transmitter and receiver coils are also difficult to maintain the correct state at all times, and the efficiency also decreases as the distance between them increases [10]. These problems have largely limited the scope of application of WPT. In order to solve these problems, lots of scholars have made some improvement solutions after continuous exploration in recent years. In [11], a scheme of adding autonomous steering alignment in an electric vehicle wireless charging system has been proposed, which can effectively reduce power fluctuations caused by coil misalignment. It proposes to compensate for the power loss caused by the vehicle position shift by adjusting the primary side power and current values in the electric vehicle dynamic wireless power transfer system in [12]. Reference [13] uses a hollow metal

The associate editor coordinating the review of this manuscript and approving it for publication was Atif Iqbal.

This work is licensed under a Creative Commons Attribution 4.0 License. For more information, see http://creativecommons.org/licenses/by/4.0/

structure to generate a uniform magnetic field, so that the load in any position in the test chamber can receive stable electric energy, but the power transfer range is limited by the metal structure, and the efficiency is only higher than 50%. The research team of S. Y. Ron Hui of the University of Hong Kong has proposed a series of 2D and 3D WPT systems based on multi-transmitting coils for a full range of WPT [14]–[17], but these systems all rely on load detection technology, and the control method is complex, moreover the practicality is not high. Jungsik Kim uses impedance matching technology to achieve efficient WPT over a wide range, but with complex circuit structures and limited computational accuracy [18]. Assawaworrarit et al. introduced the concept of parity time (PT) symmetry from quantum physics [19]. When the dynamic model of the WPT system satisfies the PT symmetry condition, the energy stored in the transmitting and receiving resonators will remain equal in the exact PT symmetry region, and the transmitting efficiency will remain constant over the range of variation of the coupling coefficient [19]–[22]. However, the WPT system using the operational amplifier to achieve nonlinear PT in the literature [19] has an output power of only 19.7 mW and an efficiency of less than 10%, which cannot be practically applied. In [23], based on [19], the power electronic converter is used to construct the nonlinear saturation gain negative resistance, which greatly improves the power level of the WPT system, but still only 10W, and without considering the working efficiency of the high-frequency inverter circuit when the frequency is bifurcated, and only the ability of the WPT system to resist changes in transfer distance has been studied. In actual industrial production activities, the output power of the wireless charging station should be large enough to meet job requirements and the charging position of logistic robots needs to be designed to be freer, and the effective charging area is as large as possible to meet its work requirements. Therefore, it is necessary to discuss the working principle of the WPT system for the load position and directionality problems.

In this paper, a time-varying coupled-mode model of WPT system with PT symmetry principle is proposed based on the direction offset angle of the receiver coil, and is applied to the distributed wireless charging system of logistic robots. The reminder of this paper is arranged as follows: In Section II, the variation law of coupling coefficient is expounded in detail. Then the modeling and characteristics of the time-varying coupled-mode model of WPT system are analyzed in Section III. Section IV present the experimental verification of the WPT system for a logistic robot, and experimental results from a prototype built in the lab are provided. Finally, some conclusions are given in the Section V.

II. COUPLING COEFFICIENT WITH VARYING SPATIAL

A. STRUCTURE OF TRANSMITTER AND RECEIVER COILS

In the wireless power transfer system for logistic robots, the weight and volume of the transmitter and receiver coils should be as small as possible, so as to reduce the adverse effects of limited working area and reduced load capacity of the logistic robots due to the excessive coils. Considering that the circular coils have a smaller volume and mass, which can save the space of the charging station, and will not add more additional burden to logistic robots from the receiver coil itself. Therefore, this paper uses two planar spiral coils without magnetic core as the transmitter and receiver coils of the WPT system, which has the advantages of small size, light weight, and low cost. The sectional view of the circular coil's structure is shown in Fig. 1.

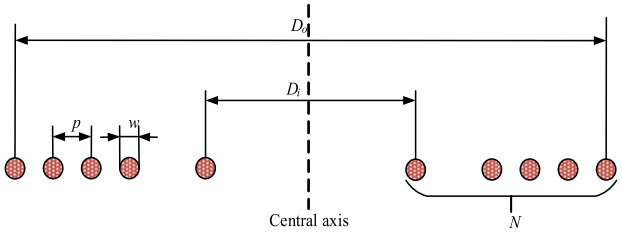

FIGURE 1. The sectional view of a circular spiral structure.

In Fig. 1, p is the pitch of the center of adjacent wires, w is the wire diameter, N is the number of turns, D_o is the outer diameter of the planar circular spiral coil, D_i is the inner diameter of the planar circular spiral coil, and $D_i = D_o - 2(N-1)p$.

The self-inductance calculation formula of single-layer planar spiral coil is [24]

$$\begin{cases} L = \dfrac{C_1 \mu_0 N^2 D_{avg}}{2}\left(\ln\dfrac{C_2}{\xi} + C_3\xi + C_4\xi^2\right) \\ D_{avg} = \dfrac{D_o + D_i}{2} \\ \xi = \dfrac{D_o - D_i}{D_o + D_i} \end{cases} \tag{1}$$

In high-frequency applications, due to the skin effect and proximity effect, the internal resistance of the coil is mainly determined by the AC resistance, and the higher the frequency, the greater the AC resistance [25]. Let the wire's diameter $w = 1.5$mm, number of turns $N = 21$, and perform FEM simulation by changing the parameters such as inside diameter of the coil D_i and spacing p. The AC resistance of the coil is shown in Fig. 2. It can be seen that as the coil inner diameter increases, its AC resistance will increase, that is, the larger the coil size, the greater its AC resistance. On the other hand, when the turn spacing is small, the AC resistance is large. At this time, the influence of the proximity effect is obvious. As the turn spacing increases, the AC resistance gradually decreases, or even tends to remain unchanged. Therefore, in the design of the coil, the skin effect and the proximity effect under high frequency should be fully considered to minimize the AC resistance of the coil to improve the transmitting efficiency of the system.

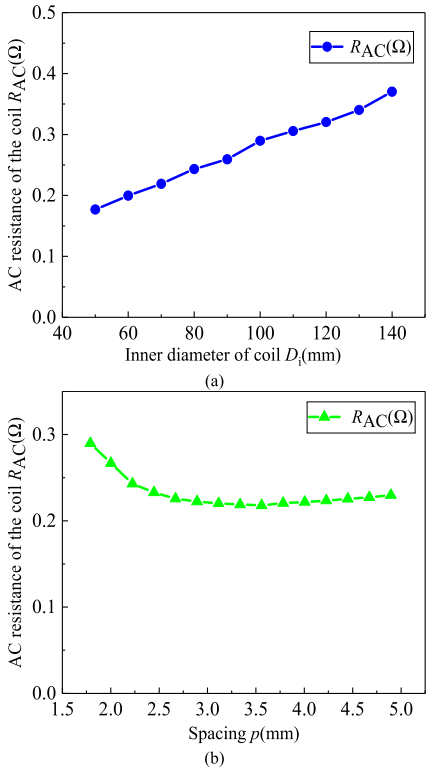

FIGURE 2. The AC resistance of the coils: (a) with varying inner diameter of coil D_i; (b) with varying spacing p.

TABLE 1. Theoretical parameters of coils.

Parameters	Tx Coil	Rx Coil
Outer diameter D_o (mm)	260	260
Number of turns N	21	26
Spacing p (mm)	1.5	1.5
Wire diameter w (mm)	1.5	1.5
Inside diameter D_i (mm)	200	185
Internal resistance R_{AC} (Ω)	0.55	0.65
Self-inductance L (μH)	182.7	247.9

Assuming that the natural resonant frequency of the coil is $f = 300$ kHz, the skin depth is

$$\Delta\varsigma = \sqrt{\frac{1}{\pi\sigma f\mu_0}} \tag{2}$$

Considering the skin effect, the diameter of a single strand should be less than $2\Delta\varsigma$, and the proximity effect at high frequencies will increase the AC impedance of the wire. Therefore, both the transmitter and receiver coils are selected as Φ0.05mm*400 polyester silk bag Litz line. The specific design values are shown in Table 1.

B. COUPLING COEFFICIENT BETWEEN TRANSMITTER AND RECEIVER COILS

The spatial arbitrary position of the two planar coils is shown in Fig. 3. At this time, the mutual inductance calculation formula of the two single circular coils is [26]:

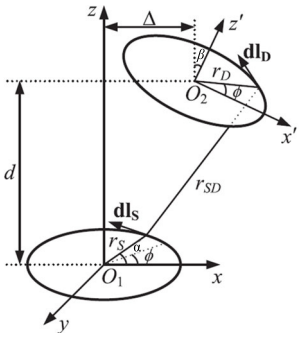

FIGURE 3. Any position of the two planar coils.

$$M_{SD}(r_S, r_D, d, \Delta, \beta) = \frac{\mu_0 r_S r_D}{4\pi}\oint d\phi \oint \frac{\sin\alpha\sin\phi\cos\beta + \cos\alpha\cos\phi}{r_{SD}(r_S, r_D, d, \Delta, \beta, \alpha, \phi)} d\alpha \tag{3}$$

wherein,

$$\begin{aligned} r_{SD}(r_S, r_D, d, \Delta, \beta, \alpha, \phi) &= [r_S^2 + r_D^2 + d^2 + \Delta^2 + 2r_D\Delta\cos\phi\cos\beta \\ &\quad - 2r_S\Delta\cos\alpha - 2r_S r_D(\cos\alpha\cos\phi\cos\beta + \sin\alpha\sin\phi) \\ &\quad - 2r_D d\cos\phi\sin\beta]^{\frac{1}{2}} \end{aligned} \tag{4}$$

r_S and r_D are the radii of two single-turn coils, d is the axial distance between the centers of the two coils, Δ is the horizontal lateral shift distance between the centers of the two coils, and β is the angle between the normal directions of the two coils. For the mutual inductance between the two planar circular spiral coils with the number of turns N_1 and N_2, the outer diameters D_{o1} and D_{o2}, and the spacing respectively p_1 and p_2, respectively, the equations (3) and (4) can be used to find the mutual inductance. The mutual inductance between each circular coil is finally superimposed to

$$M(N_1, N_2, D_{o1}, D_{o2}, p_1, p_2, d, \Delta, \beta) = \sum_{i=1}^{N_1}\sum_{j=1}^{N_2} M_{SD}\left(D_{o1}/2-(i-1)p_1, D_{o2}/2-(j-1)p_2, d, \Delta, \beta\right) \tag{5}$$

As for a WPT system through magnetic field coupling, the natural resonant frequency f of the coupled coils, the load R_L and the mutual inductance M between the coils are the main factors affecting the effective transfer characteristics of the power. For the actual WPT system used for logistic robots, the mutual inductance M directly determines the characteristics of the WPT system when the natural resonant frequency f and the load resistance of the coil R_L are constant. And the mutual inductance M is also determined by many factors. Wherein, the direction of the offset between the coils is one of the main factors. Therefore, by studying the influence of the coil offset angle on the mutual inductance between the coils, the influence on the power transfer characteristics of the WPT system can be obtained.

Therefore, this paper mainly considers the influence of the relative position of the two planar coils on the proposed system. That is, the coupling coefficient of the proposed system is a function of a certain offset angle β of the receiver coil with respect to the center of the transmitter coil:

$$k_{12}(\beta) = \frac{M\left(N_1, N_2, D_{o1}, D_{o2}, p_1, p_2, d, \Delta, \beta\right)}{\sqrt{L_1 L_2}} \tag{6}$$

The magnetic field simulation software JMAG, which is commonly used in industry, is used to simulate the characteristics of magnetic field changes of the coupling mechanism designed in this paper. The magnetic field distribution of the two coils is obtained in different directions, as shown in Fig. 4. It can be seen that when the relative positions of the receiver coil and the transmitter coil change, the distribution of the magnetic field around them changes accordingly. Wherein, when the coils are in an axially symmetrical position, the magnetic fields around them are uniformly distributed. When there is a certain radial offset distance or axial offset angle between the coils, for instance in the same plane or perpendicular to each other, the magnetic fields around coils are no longer evenly distributed, but closely related to their relative positions. So, we can get the conclusion that the change of the relative position between the coils has a great influence on the magnetic field distribution around the space.

Fig. 5 shows influence of offset angle and transmission distance on mutual inductance. When the transmission distance is smaller and the direction deviation angle is smaller, the mutual inductance value is larger, and on the contrary, the mutual inductance value is smaller. It is worth mentioning that, when the direction deviation angle tends to 90°, the mutual inductance also tends to 0.

In the actual scene of WPT system for logistic robots, the two typical coil positions of axial movement with an offset of 0° and radial movement with an offset of 90° are selected, and the variation law of coupling coefficient between coils is studied, as shown in Fig. 6, including the comparison between calculated, simulated and actual measured results. It can be seen from Fig.6 that as the relative positions of the

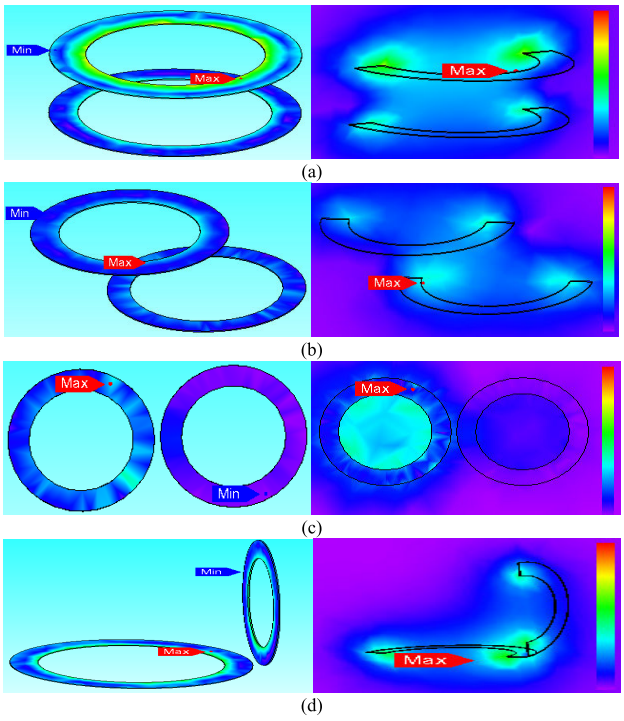

FIGURE 4. Magnetic field distribution trait with varying spatial: (a) axial alignment; (b) radial offset; (c) 180° offset; (d)90° offset.

two coils change, the coupling coefficient will also change accordingly. Obviously, this is very disadvantageous for the conventional WPT system based on the magnetic coupling principle. In practical applications, the WPT system must have sufficient capacity to resist the obstacles caused by this change in coupling coefficient, which be able to bring practical value.

III. MODELING AND ANALYSIS OF SYSTEM

A. COUPLED-MODE MODELING

The circuit topology of the WPT system based on parity time symmetry principle is shown in Fig. 7(a), in which the negative resistance - R is used as a power source to provide energy for the system, and the phase of the negative resistance's

$$\begin{bmatrix} \frac{\mathrm{d}i_{L1}}{\mathrm{d}t} \\ \frac{\mathrm{d}u_{C1}}{\mathrm{d}t} \\ \frac{\mathrm{d}i_{L2}}{\mathrm{d}t} \\ \frac{\mathrm{d}u_{C2}}{\mathrm{d}t} \end{bmatrix} = \begin{bmatrix} -\frac{L_2 r_1}{L_1 L_2 - [M_{12}(\beta)]^2} & -\frac{L_2}{L_1 L_2 - [M_{12}(\beta)]^2} & \frac{M_{12}(\beta)\,(r_2 + R_L)}{L_1 L_2 - [M_{12}(\beta)]^2} & \frac{M_{12}(\beta)}{L_1 L_2 - [M_{12}(\beta)]^2} \\ \frac{1}{C_1} & 0 & 0 & 0 \\ \frac{M_{12}(\beta) r_1}{L_1 L_2 - [M_{12}(\beta)]^2} & \frac{M_{12}(\beta)}{L_1 L_2 - [M_{12}(\beta)]^2} & -\frac{L_1\,(r_2 + R_L)}{L_1 L_2 - [M_{12}(\beta)]^2} & -\frac{L_1}{L_1 L_2 - [M_{12}(\beta)]^2} \\ 0 & 0 & \frac{1}{C_2} & 0 \end{bmatrix} \cdot \begin{bmatrix} i_{L1} \\ u_{C1} \\ i_{L2} \\ u_{C2} \end{bmatrix} + \begin{bmatrix} \frac{L_2}{L_1 L_2 - [M_{12}(\beta)]^2} \\ 0 \\ -\frac{M_{12}(\beta)}{L_1 L_2 - [M_{12}(\beta)]^2} \\ 0 \end{bmatrix} v_o \tag{7}$$

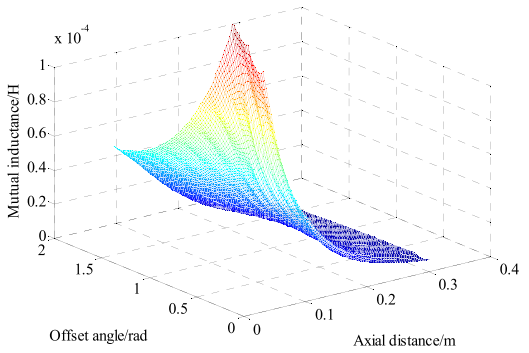

FIGURE 5. Influence curve of offset angle and transmission distance on mutual inductance.

output voltage and output current proposed in this paper are always the same as Fig. 7(b), which is exactly the opposite of the positive resistance absorption power. The direction change amount of coil's position is added to the static system in which the coil is axially symmetrically placed, so that a time-varying coupled-mode model of WPT system based on the offset angle of the receiver coil is proposed.

For the system shown in Fig. 6, the space state equation can be obtained

Introducing complex variables

$$\begin{cases} a_{1\pm} = \sqrt{\dfrac{L_1}{2}}\left(i_{L1} \pm \mathrm{j}\sqrt{\dfrac{C_1}{L_1}}u_{c1}\right) \\ a_{2\pm} = \sqrt{\dfrac{L_2}{2}}\left(i_{L2} \pm \mathrm{j}\sqrt{\dfrac{C_2}{L_2}}u_{c2}\right) \end{cases} \tag{8}$$

Then $|a_1|^2$ and $|a_2|^2$ characterize the energy stored in the energy storage element of the transmitter resonant circuit and the receiver resonant circuit, respectively.

The relationship between the coupled mode and the state variable is [23]

$$\boldsymbol{a}_n = \sqrt{\frac{L_n}{2}}i_{Ln} + j\sqrt{\frac{C_n}{2}}u_{Cn} = A_n e^{j(\omega t+\theta_n)} \tag{9}$$

Among them, the amplitude A_n and the phase angle θ_n are slowly varying amounts on the time scale $\tau = \omega t$, thus satisfying $dA_n/dt \ll \omega$, $d\theta_n/dt \ll \omega$.

For the WPT system shown in Fig. 6, the natural resonant frequencies of the transmitter and receiver are respectively $\omega_1 = \sqrt{L_1C_1}$ and $\omega_2 = \sqrt{L_2C_2}$, the inherent loss rate is $\Gamma_{10} = r_1/2L_1$ and $\Gamma_{20} = r_2/2L_2$, loss rate due to load as $\Gamma_L = R_L/2L_2$, coupling coefficient is $k_{12}(\beta) = M_{12}(\beta)/\sqrt{L_1L_2}$. Since the operating frequency of the system power supply is very high, A_1, A_2, θ_1 and θ_2 are relatively slow variables of time. When their value changes by one cycle, the number of cycles through which the power supply passes is much larger than 1. Therefore, according to the principle of averaging, it is available by combing (7)∼(9)

$$\frac{dA_1}{dt} = -\frac{1}{1-[k_{12}(\beta)]^2}\Gamma_{10}A_1$$

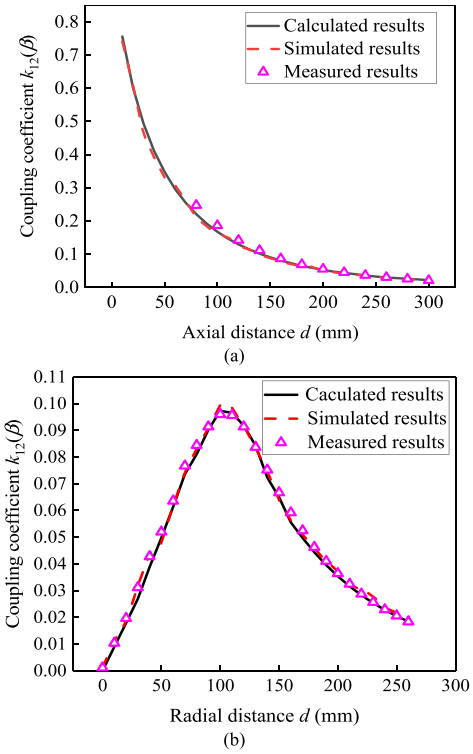

FIGURE 6. Coupling coefficient between two coils at different positions: (a) axial movement with an offset of 0° and (b) radial movement with an offset of 90°.

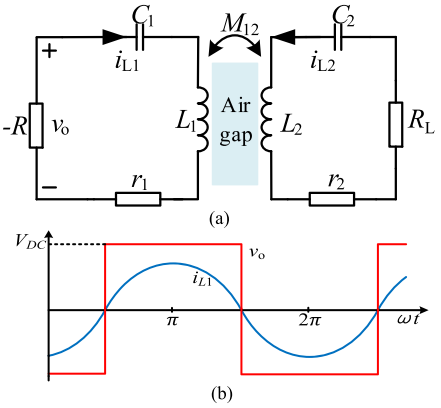

FIGURE 7. The WPT system based on parity time symmetry principle: (a) the circuit topology and (b) the current-voltage relationship of the nonlinear negative resistance.

$$\begin{aligned} &-\frac{1}{2}\frac{k_{12}(\beta)}{1-[k_{12}(\beta)]^2}\omega_2 A_2\sin(\theta_1-\theta_2) \\ &+\frac{1}{1-[k_{12}(\beta)]^2}(\Gamma_{10}+\Gamma_L)A_2\cos(\theta_1-\theta_2) \\ &+\frac{1}{\sqrt{2L_1}}\frac{1}{1-[k_{12}(\beta)]^2}\frac{2V_{DC}}{\pi} \\ A_1&\left(\omega+\frac{d\theta_1}{dt}\right) \\ &=\frac{1}{2}\omega_1 A_1+\frac{1}{2}\frac{1}{1-[k_{12}(\beta)]^2}\omega_1 A_1 \end{aligned} \tag{10}$$

$$
\begin{aligned}
&-\frac{1}{2}\frac{k_{12}(\beta)}{1-[k_{12}(\beta)]^2}\omega_2 A_2\cos(\theta_1-\theta_2)\\
&-\frac{1}{1-[k_{12}(\beta)]^2}(\Gamma_{20}+\Gamma_{\mathrm{L}})A_2\sin(\theta_1-\theta_2) \qquad (11)\\
\frac{dA_2}{dt}=&-\frac{1}{1-[k_{12}(\beta)]^2}(\Gamma_{20}+\Gamma_{\mathrm{L}})A_2\\
&+\frac{1}{2}\frac{k_{12}(\beta)}{1-[k_{12}(\beta)]^2}\omega_1 A_1\sin(\theta_1-\theta_2)\\
&+\frac{k_{12}(\beta)}{1-[k_{12}(\beta)]^2}\Gamma_{10}A_1\cos(\theta_1-\theta_2)\\
&-\frac{1}{\sqrt{2L_1}}\frac{k_{12}(\beta)}{1-[k_{12}(\beta)]^2}\frac{2V_{\mathrm{DC}}}{\pi}\cos(\theta_2-\theta_1) \qquad (12)\\
A_2&\left(\omega+\frac{d\theta_2}{dt}\right)\\
=&\frac{1}{2}\omega_2 A_2+\frac{1}{2}\frac{1}{1-[k_{12}(\beta)]^2}\omega_2 A_2\\
&-\frac{1}{2}\frac{k_{12}(\beta)}{1-[k_{12}(\beta)]^2}\omega_1 A_1\cos(\theta_1-\theta_2)\\
&+\frac{k_{12}(\beta)}{1-[k_{12}(\beta)]^2}\gamma_1 A_1\\
&\sin(\theta_1-\theta_2)+\frac{1}{\sqrt{2L_1}}\frac{k_{12}(\beta)}{1-[k_{12}(\beta)]^2}\\
&\frac{2V_{\mathrm{DC}}}{\pi}\sin(\theta_2-\theta_1) \qquad (13)
\end{aligned}
$$

At this point, select the complex variable $\boldsymbol{a_n}$ as the new state variable, and then the space state equation can be written as

$$
\frac{d\boldsymbol{a}_n}{dt}=\frac{dA_n}{dt}e^{j(\omega t+\theta_n)}+jA_n\left(\omega+\frac{d\theta_n}{dt}\right)e^{j(\omega t+\theta_n)} \qquad (14)
$$

Therefore, the new system state equation can be obtained:

$$
\begin{cases}
\dfrac{\mathrm{d}\boldsymbol{a}_1}{\mathrm{d}t}\\
=\left[\begin{array}{l}\dfrac{1}{\sqrt{2L_1}}\dfrac{1}{1-[k_{12}(\beta)]^2}\dfrac{2V_{\mathrm{DC}}}{\pi}\dfrac{1}{|\boldsymbol{a}_1|}-\dfrac{1}{1-[k_{12}(\beta)]^2}\Gamma_{10}\\ \quad+j\dfrac{1}{2}\omega_1\left(1+\dfrac{1}{1-[k_{12}(\beta)]^2}\right)\end{array}\right]\boldsymbol{a}_1\\
\quad+\left[\dfrac{k_{12}(\beta)}{1-[k_{12}(\beta)]^2}(\Gamma_{20}+\Gamma_{\mathrm{L}})-j\dfrac{1}{2}\dfrac{k_{12}(\beta)}{1-[k_{12}(\beta)]^2}\omega_2\right]\boldsymbol{a}_2\\
\dfrac{\mathrm{d}\boldsymbol{a}_2}{\mathrm{d}t}\\
=\left[\begin{array}{l}\dfrac{k_{12}(\beta)}{1-[k_{12}(\beta)]^2}\Gamma_{10}-j\dfrac{1}{2}\dfrac{k_{12}(\beta)}{1-[k_{12}(\beta)]^2}\omega_1\\ -\dfrac{1}{\sqrt{2L_1}}\dfrac{k_{12}(\beta)}{1-[k_{12}(\beta)]^2}\dfrac{2V_{\mathrm{DC}}}{\pi}\dfrac{1}{|\boldsymbol{a}_1|}\end{array}\right]\boldsymbol{a}_1\\
\quad+\left[-\dfrac{1}{1-[k_{12}(\beta)]^2}(\Gamma_{20}+\Gamma_{\mathrm{L}})\right.\\
\quad\left.+j\frac{1}{2}\omega_2\left(1+\frac{1}{1-[k_{12}(\beta)]^2}\right)\right]\boldsymbol{a}_2
\end{cases} \qquad (15)
$$

According to the coupled-model modeling condition $\omega_1=\omega_2=\omega_0$, assuming that the system is in a weakly coupled state, the inductive coupling coefficient is small, i.e. $k_{12}(\beta)\ll 1$. Under this condition, there is 1-$[k_{12}(\beta)]^2\approx 1$ in (15). In addition, ignoring the second-order small quantity, the coupled mode equation of the system is finally obtained

$$
\begin{cases}
\dfrac{\mathrm{d}\boldsymbol{a}_1}{\mathrm{d}ty}=\left[\dfrac{1}{\sqrt{2L_1}}\dfrac{2V_{\mathrm{DC}}}{\pi}\dfrac{1}{|\boldsymbol{a}_1|}-\Gamma_{10}+j\omega_0\right]\boldsymbol{a}_1\\
\qquad -j\frac{k_{12}(\beta)}{2}\omega_0\,\boldsymbol{a}_2\\
\dfrac{\mathrm{d}\boldsymbol{a}_2}{\mathrm{d}ty}=-j\dfrac{k_{12}(\beta)}{2}\omega_0\boldsymbol{a}_1+[-(\Gamma_{20}+\Gamma_{\mathrm{L}})+j\omega_0]\,\boldsymbol{a}_2
\end{cases} \qquad (16)
$$

B. CHARACTERISTIC ANALYSIS

The item $\frac{1}{\sqrt{2L_1}}\frac{2V_{\mathrm{DC}}}{\pi}\frac{1}{|\boldsymbol{a}_1|}-\Gamma_{10}$ in (16) can be denoted as g_1. Therefore, when the system enters a steady state, it can be obtained by (16)

$$
\begin{vmatrix}
[g_1+j(\omega-\omega_0)] & j\dfrac{k_{12}(\beta)}{2}\omega_0\\
j\dfrac{k_{12}(\beta)}{2}\omega_0 & [j(\omega-\omega_0)+(\Gamma_{20}+\Gamma_{\mathrm{L}})]
\end{vmatrix}=0 \qquad (17)
$$

Therefore, the steady-state solution expression of the operating frequency ω and the energy modes $|a_1(\beta)|$, $|a_2(\beta)|$ of the system operating in the symmetrical or antisymmetric state can be obtained by (17)

$$
\begin{cases}
\omega=\omega_0\mp\sqrt{(\dfrac{k_{12}(\beta)\omega_0}{2})^2-(\Gamma_{20}+\Gamma_{\mathrm{L}})^2}\\
|\boldsymbol{a}_1(\beta)|\big/|\boldsymbol{a}_2(\beta)|=1\\
|\boldsymbol{a}_2(\beta)|=\dfrac{1}{\Gamma_{10}+\Gamma_{20}+\Gamma_{\mathrm{L}}}\dfrac{1}{\sqrt{2L_1}}\dfrac{2V_{\mathrm{DC}}}{\pi}
\end{cases} \qquad (18)
$$

wherein, the condition $k_{12}(\beta)\omega_0/2\geq\Gamma_{20}+\Gamma_{\mathrm{L}}$ must be meet to ensure that the operating frequency ω is a real number. Therefore, we can judge whether the system works in the PT symmetry or antisymmetric state by whether the condition is true or not.

According to the coupled mode theory, the output power expression is

$$
P_{\mathrm{L}}=2\Gamma_{\mathrm{L}}|a_2|^2 \qquad (19)
$$

Substituting the value of $|a_2(\beta)|$ in (18) into (19), the system output power expression when the modified model satisfies the PT symmetry condition is

$$
P_{\mathrm{L}}=\frac{\Gamma_{\mathrm{L}}}{[\Gamma_{10}+(\Gamma_{20}+\Gamma_{\mathrm{L}})]^2}\frac{4V_{\mathrm{DC}}^2}{L_1\pi^2} \qquad (20)
$$

For a single-load WPT system, the transmitting efficiency expression is

$$
\eta=\frac{2\Gamma_{\mathrm{L}}|a_2|^2}{2\Gamma_{10}|a_1|^2+(\Gamma_{20}+\Gamma_{\mathrm{L}})|a_2|^2}\times 100\% \qquad (21)
$$

Therefore, the system transmitting efficiency expression when the modified model satisfies the PT symmetry condition is

$$
\eta=\frac{\Gamma_{\mathrm{L}}}{\Gamma_{10}+\Gamma_{20}+\Gamma_{\mathrm{L}}}\times 100\% \qquad (22)
$$

Therefore, conclusions can be drawn from (20) and (22), that when the proposed system operates in the PT symmetrical or anti symmetrical state, that is, the condition

$k_{12}(\beta)\omega_0/2 \geq \Gamma_{20} + \Gamma_L$ is satisfied, the output power and transmitting efficiency of the system are not affected by the offset angle β of the coil's position. So, we can define the working area of this feature as a PT symmetry range. Fig. 8 shows the variation of system characteristics with the coupling coefficient $k_{12}(\beta)$.

It can be seen that when the system works in the PT symmetry range, each coupling coefficient corresponds to two operating frequencies, that is, the system will run at the frequency of one of the PT symmetric solution or the antisymmetric solution, and at this time, the output power and efficiency of the proposed system do not change with the change of the coupling coefficient $k_{12}(\beta)$, and maintain a constant value. Otherwise, when the coupling coefficient $k_{12}(\beta)$ is less than the critical value, that is, the condition $k_{12}(\beta)\omega_0/2 \geq \Gamma_{20} + \Gamma_L$ is not satisfied, the proposed system characteristics are restored to the characteristics of the conventional MCR-WPT, that is, the operating frequency of the system no longer varies with the coupling coefficient, but is stabilized at the natural resonant frequency, and the output power and efficiency vary with the mutual inductance, and there is only one working point with the highest output power, but its efficiency is only 50%.

C. MOVABLE PERFORMANCE

The WPT system designed in this paper will be applied in the field of logistic robots. For such loads with movable features, the random change of mutual inductance is the most critical factor which will affect the performance of WPT system. Not only is there a disturbance from the load position offset to the system, but the moving speed of the load also causes the mutual inductance to be unstable. Therefore, the impact of the speed of the load on the entire WPT system is also worth exploring.

The KVL equation for the receiver circuit of the WPT system shown in Fig.7(a) can be described by

$$j\omega M_{12}(\beta)\dot{I}_{L1} + (R_L + r_2)\dot{I}_{L2} + j\omega L_2\dot{I}_{L2} - j\frac{1}{\omega C_2}\dot{I}_{L2} = 0 \tag{23}$$

The voltage v_2 across the receiver coil can be expressed as

$$\begin{aligned} v_2 &= \frac{d}{dt}(M_{12}(\beta)i_{L1} + L_2 i_{L2}) \\ &= \mathrm{M}_{12}(\beta)\frac{d}{dt}i_{L1} + i_{L1}\frac{dM_{12}(\beta)}{dx}\frac{dx}{dt} + L_2\frac{d}{dt}i_{L2} + i_{L2}\frac{d}{dt}Ly_2 \end{aligned} \tag{24}$$

When the logistic robot moves, it can be seen from Fig. 6 that the mutual inductance $M_{12}(\beta)$ and its rate of change $\mathrm{d}M_{12}(\beta)/\mathrm{d}t$ are all changed at any time, but the self-inductance of the receiver coil is its inherent property, that is, $\mathrm{d}L_2/\mathrm{d}t = 0$. Assuming that the current i_{L1} of transmitter coil and the current i_{L2} of the receiver coil are both sinusoidal signals at steady state, and the speed of the logistic robot is expressed as $V = \mathrm{d}x/\mathrm{d}t$ per unit time, then (24) can be

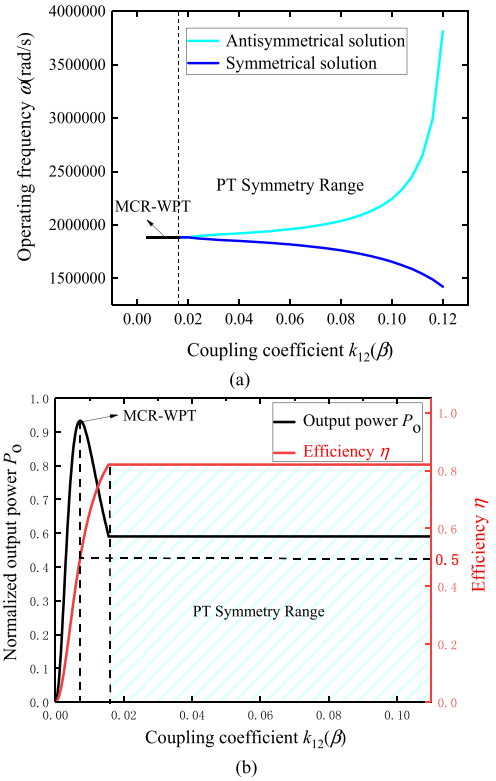

FIGURE 8. Transfer performance of the proposed system: (a) operating frequency and (b) output power & efficiency.

rewritten as

$$V_2 = j\omega M_{12}(\beta)I_{L1} + I_{L1}V\frac{dM_{12}(\beta)}{dx} + j\omega L_2 I_{L2} \tag{25}$$

The second term is the effect of load movement in (25), which just happens to reflect the move characteristics of the load, i.e. V represents the moving speed of the logistic robot, and $\mathrm{d}M_{12}(\beta)/\mathrm{d}x$ reflects the real-time location of the logistic robot.

This paper sets the inherent resonant frequency of the coil $f_0 = 300\mathrm{kHz}$. According to (18), the operating frequency of the full-bridge inverter circuit will vary up and down at this natural resonant frequency. So, the operating frequency $f = 300\mathrm{kHz}$ can be taken, and the moving speed of the logistic robot is $V = 15\mathrm{km/h}$. According to Fig. 5(a), when the mutual inductance $M = 21.6\mu\mathrm{H}$, the rate of change can be approximated as $\mathrm{d}M_{12}(\beta)/\mathrm{d}x = 14.4\mu\mathrm{H/m}$, then

$$\left|I_{L1}\frac{dx}{dt}\cdot\frac{dM_{12}(\beta)}{dx}\right| \Big/ |j\omega M_{12}(\beta)I_{L1}| \approx 0 \tag{26}$$

Therefore, in the three constituent units of (25), the second term representing the load-moving characteristic accounts for a close to zero, which means that the voltage across the receiver coil at any time is substantially independent of the movement of the load. In other words, the moving speed of logistic robots does not affect the wireless charging system for them.

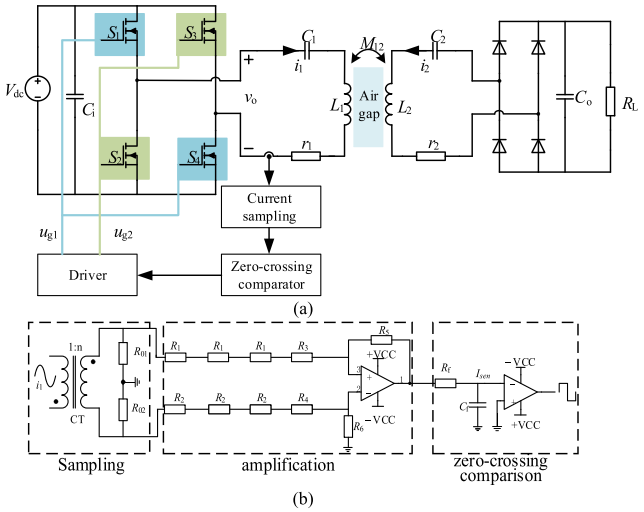

FIGURE 9. System circuit implementation: (a) the main circuit and (b) sampling amplification & zero-crossing comparison circuit.

IV. EXPERIMENTAL VERIFICATIONS

A. NEGATIVE RESISTANCE IMPLEMENTATION

In order to realize the characteristics of the model mentioned in section III, the high-frequency AC power supply of the WPT system should satisfy the characteristics of the negative resistance as shown in Fig. 7(b). It is necessary to emphasize in particular that this paper differs from [19] in that the negative resistance is achieved with a power electronic converter, so that it can provide enough energy for efficient and stable wireless charging for logistic robots.

The inverter circuit of the proposed model selects the full-bridge topology, and the control circuit is composed of a sampling amplifying circuit, a zero-crossing comparison circuit and a driving circuit, as shown in Fig. 9. The working principle is that the sinusoidal current signal of the transmitter coil is sampled by the current transformer and converted into a voltage signal firstly, and then amplified by a differential amplifying circuit to output the signal. Finally, the signal passes through a zero-crossing comparator and generates two complementary PWM signals via a logic circuit.

Since the PWM signals output by the comparator with a weak driving capability by the characteristics of low voltage and small current, but the gate voltage of the selected Power MOSFET Infineon-BSC160N10NS3 is $12 \sim 20$V, the PWM signals have to be amplified by the driving circuit to drive the Power MOSFET. This article uses four Silicon Labs SI8271 isolated driver chips to provide drivers for the full-bridge inverter circuit.

B. HARDWARE IMPLEMENTATION

According to the theoretical results, the experimental prototype was built as shown in Fig. 10. Among them, in addition to the transmitter and receiver coils are already introduced, the 50V DC input voltage is provided by the KXN-10010D DC power supply, the switches of the full-bridge inverter circuit are four Power MOSFET BSC160N10NS3 from

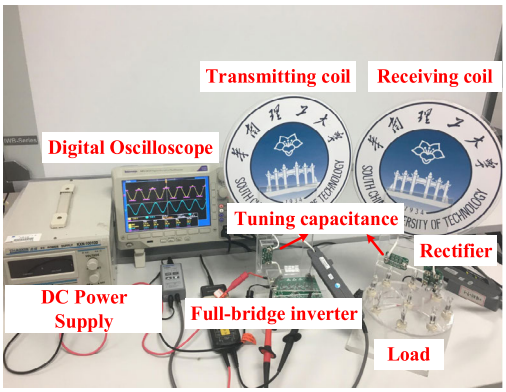

FIGURE 10. Experimental prototype proposed in this paper.

TABLE 2. Parameters of the experimental prototype.

Symbol	Note	Values
V_{dc}	Input voltage	50 V
L_1	Transmitter inductance	185.12 μH
L_2	Receiver inductance	252.28 μH
C_1	Transmitter capacitance	1527.8 pF
C_2	Receiver capacitance	1121.8 pF
r_1	Transmitter equivalent resistance	590 mΩ
r_2	Receiver equivalent resistance	650 mΩ
f_1	Transmitter resonant frequency	300 kHz
f_2	Receiver resonant frequency	300 kHz
R_L	Equivalent load resistance	16.667 Ω
R_D	Mosfet equivalent resistance	0.180 Ω
R_d	Diode equivalent resistance	0.2 Ω

Infineon, and there are four isolated driver chips named SI8271 from Silicon Labs to control the switch on and off, the full-bridge rectifier circuit on the receiver side consists of four Schottky diodes V15PM15, the current is measured using a current amplifier CYBERTEK CP0030H, the voltage is measured using a voltage isolation probe Tektronix P5200A, and all experimental waveforms are obtained by a Tektronix DPO3014 Digital Oscilloscope. At the same time, the coupling coils is placed on a bracket with a height of 20cm to eliminate the influence of the iron table. In order to facilitate the recording of measured results and visual display of them, the load used an array of halogen bulbs instead of a logistic robot.

The experimental parameters used in this paper are shown in Table 2, since the coils are all wound by hand, there is a certain error between the actual value of the coil parameter and the theoretical value.

In order to confirm the correctness and practicability of the WPT system proposed in this paper, relevant tests were carried out in the laboratory using the prototype shown in Fig. 10. According to the analysis of the characteristics of the proposed model in III, when the coupling coefficient satisfies $k_{12}(\beta)\omega_0/2 \geq \Gamma_{20}+\Gamma_L$, the performance of the WPT system will be independent of the offset angle between the coils, thus maintaining constant output power and constant transmitting efficiency, and the operating frequency is no longer the natural resonant frequency of the coupling mechanism, but one of a symmetric solution or an asymmetric solution

TABLE 3. Transfer performance of the proposed system.

Positional relationship	i_1/A	i_2/A	Operating frequency/kHz	Output power/W	Transmitting efficiency
Axial alignment	3.88	3.34	289.1	150.92	90.7%
Radial offset	3.89	3.37	286.3	150.48	90.1%
180°offset	3.78	3.29	295.7	150.41	90.0%
90°offset	3.91	3.36	288.6	150.80	90.6%

in (18). Therefore, it is convenient to judge whether the system works in the PT symmetry range by the experimental waveform or measured data of the operating frequency.

C. EXPERIMENT RESULTS

Fig. 11 shows the diagrams and corresponding main experimental waveforms when the transmitter coil and the receiver coil are in four positional relationships: axial alignment, radial offset, 180° offset and 90° offset. As you can see from the waveform chart taken on the oscilloscope, the purple line represents the output voltage v_o of the full-bridge inverter circuit, the blue line represents the current i_1 of the transmitter coil, and the cyan line represents the current i_2 of the receiver coil. It can be seen that whether the two coils are in full alignment or radial offset, or 180° offset side by side, or even 90° offset vertically, the operating frequency of the system is not the natural resonant frequency of the coupling coils. And the phase difference between the current of the transmitter coil i_1 and the current of the receiver coil i_2 is no longer 90° like the MCR-WPT's. In addition, the voltage v_o and current i_1 are substantially in phase, which indicates that the full-bridge inverter circuit achieves a negative resistance characteristic as shown in Fig. 7(b). Moreover, by reading the data on the oscilloscope, the corresponding values of output power and transmitting efficiency can be calculated as shown in Table 3. It can be seen that in these four cases, the output power of the system can be stabilized at about 150W, and the transmitting efficiency between the coils is maintained at about 90%, this shows that the system always works in the PT symmetrical area, and proves that as long as the system works in this area, it can achieve the characteristics of constant power and constant efficiency output regardless of the position and direction of the coils. This proves that the theoretical analysis conclusion in Section III, B is correct.

From the analysis in Section II, we can know that if the inherent parameters of the coils used in the WPT system have been determined, the size of the coupling coefficient between them is only related to the relative position of the coils and the angle of the offset direction. Therefore, the coupling coefficient between the coils is used as an independent variable to facilitate the experimental measurement. The specific experimental process is to keep the position of the transmitting coil unchanged, then change the relative position relationship between the receiver coil and the transmitter coil by moving the receiver coil. At the same time, measure and record the values of the coupling coefficient, operating frequency,

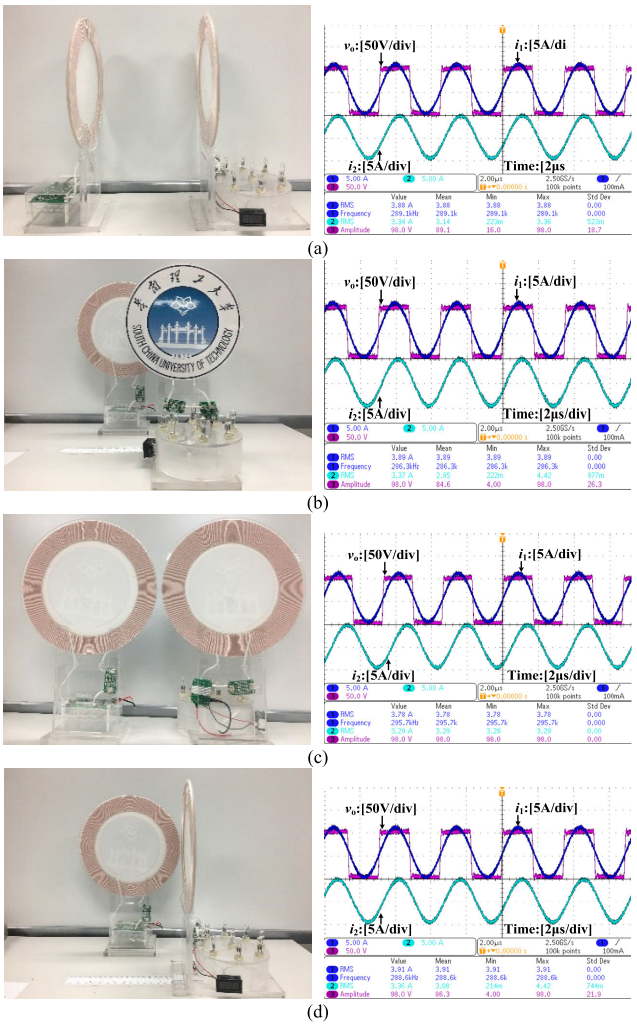

FIGURE 11. The operational waveforms of the prototype when the coils are placed in different positions:(a) axial alignment; (b) radial offset; (c) 180° offset; (d) 90° offset.

output power, and transmitting efficiency corresponding to each position, then sort according to the value of the coupling coefficient. Finally, the characteristic curves of the system based on the experimental measured data and calculated data are shown in Fig. 12.

It can be seen from the results shown in Fig. 12 that the measured results are basically consistent with the calculated results. And the critical coupling coefficient set by the experimental prototype is $k_{12}(\beta) = 0.03$, that is, when the coupling coefficient $k_{12}(\beta) \geq 0.03$, regardless of the current relative position and offset direction angle between the coils, the condition $k_{12}(\beta)\omega_0/ \geq \Gamma_{20} + \Gamma_L$ of PT symmetry range will be matched. At this time, the operating frequency of the measured results is no longer 300kHz that is the natural resonance frequency of the coils, but is mostly distributed at a higher frequency, which is the bifurcation phenomenon of IPT system. And the output power of the system is also basically stable at 150W, while the transmitting efficiency is as high as 90% within the PT symmetry range. The experimental results are in good agreement with the

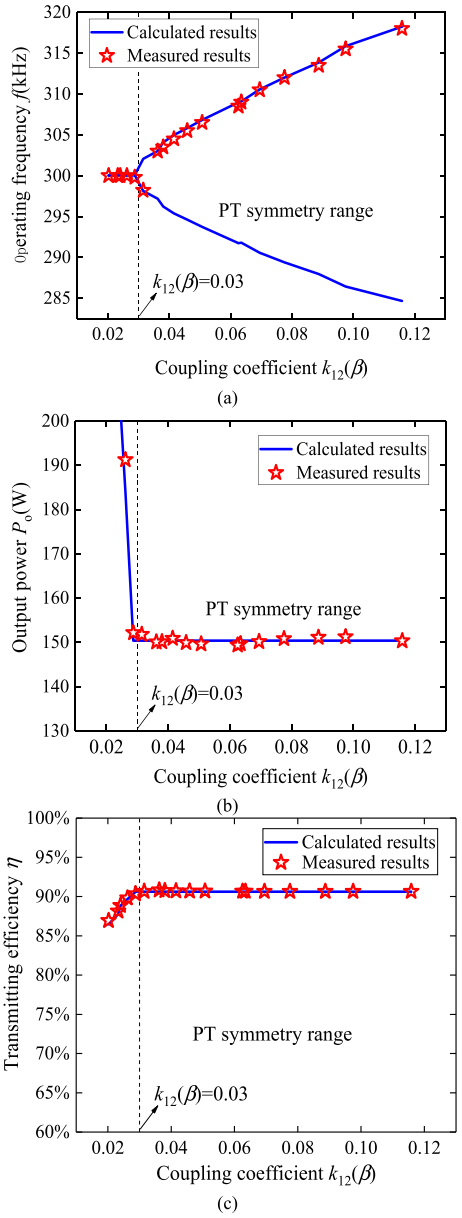

FIGURE 12. Transfer performance of the experimental prototype with dynamic movement: (a) operating frequency; (b) output power; (c) transmitting efficiency.

transfer performance of the proposed system shown in Fig. 8, which verifies the correctness of the theoretical analysis. So, when the logistic robots move at any angle and speed within a certain range around the charging station, the prototype proposed in this paper can practically provide stable power transfer with constant efficiency for it, which is independent of the change of transfer distance and offset angle of coils. In addition, it is worth mentioning that, some control methods such as the SOS PS-PWM method which is proposed in [27] can be used to make the operating frequency of IPT system meet the conditions of soft switching of the high-frequency inverter when the system has Bifurcation, thereby effectively improving the efficiency of the IPT system. Therefore, this will be explored further in our future work.

V. CONCLUSIONS

This paper proposes an omnidirectional and efficient wireless power transfer system for logistic robots based on the principle of parity time symmetry. The time-varying coupled-mode model of the system based on the offset angle of the receiver coil's position is established, wherein, the negative resistance can be realized only by controlling the current of the transmitter coil to control a full-bridge inverter circuit. In addition, by analyzing the receiver side circuit of the WPT system, the influence of the logistic robots' moving speed on the WPT system are negligible. Experimental implementation has been used for practical evaluation. The experimental results verified the WPT system proposed can realize stable 150W power transfer with constant transmitting efficiency of more than 90% for a logistic robot, which is independent of the change of transfer distance and offset angle of coils within a confined three-dimensional space around the charging station. What's more, the system's structure proposed in this paper is very simple, there is no communication circuit either DC/DC voltage regulation circuit in the output circuit on the receiver side, it can greatly reduce the complexity of the system, save the cost of construction, and is more conducive to the development of industrialization and commercialization, which provides an important guidance for logistic robots' WPT applications.

REFERENCES

[1] X. Lyu, Y. Song, C. He, Q. Lei, and W. Guo, "Approach to integrated scheduling problems considering optimal number of automated guided vehicles and conflict-free routing in flexible manufacturing systems," *IEEE Access*, vol. 7, pp. 74909–74924, 2019, doi: 10.1109/access.2019.2919109.

[2] Z. Zhang, Q. Guo, J. Chen, and P. Yuan, "Collision-free route planning for multiple AGVs in an automated warehouse based on collision classification," *IEEE Access*, vol. 6, pp. 26022–26035, 2018, doi: 10.1109/access.2018.2819199.

[3] J. Bačík, F. Ďurovský, M. Biroš, K. Kyslan, D. Perduková, S. Padmanaban, "Pathfinder–development of automated guided vehicle for hospital logistics," in *IEEE Access*, vol. 5, pp. 26892–26900, 2017, doi: 10.1109/ACCESS.2017.2767899.

[4] F. Zhang, G. Liu, and L. Fang, "Estimation of battery state of charge with H∞ observer: Applied to a robot for inspecting power transmission lines," *IEEE Trans. Ind. Electron.*, vol. 59, no. 2, pp. 1086–1095, Feb. 2012, doi: 10.1109/TIE.2011.2159691.

[5] M. Su, Z. Liu, Q. Zhu, and A. P. Hu, "Study of maximum power delivery to movable device in omnidirectional wireless power transfer system," *IEEE Access*, vol. 6, pp. 76153–76164, 2018, doi: 10.1109/access.2018.2883503.

[6] Z. Zhang, H. Pang, A. Georgiadis, and C. Cecati, "Wireless power transfer—An overview," *IEEE Trans. Ind. Electron.*, vol. 66, no. 2, pp. 1044–1058, Feb. 2018, doi: 10.1109/TIE.2018.2835378.

[7] A. P. Sample, D. A. Meyer, and J. R. Smith, "Analysis, experimental results, and range adaptation of magnetically coupled resonators for wireless power transfer," *IEEE Trans. Ind. Electron.*, vol. 58, no. 2, pp. 544–554, Feb. 2011, doi: 10.1109/tie.2010.2046002.

[8] G. A. Covic and J. T. Boys, "Modern trends in inductive power transfer for transportation applications," *IEEE J. Emerg. Sel. Topics Power Electron.*, vol. 1, no. 1, pp. 28–41, Mar. 2013, doi: 10.1109/jestpe.2013.2264473.

[9] T. Imura, H. Okabe, and Y. Hori, "Basic experimental study on helical antennas of wireless power transfer for Electric Vehicles by using magnetic resonant couplings," in *Proc. IEEE Vehicle Power Propuls. Conf.*, Sep. 2009, pp. 936–940, doi: 10.1109/vppc.2009.5289747.

[10] A. Kurs, A. Karalis, R. Moffatt, J. D. Joannopoulos, P. Fisher, and M. Soljacic, "Wireless power transfer via strongly coupled magnetic resonances," *Science*, vol. 317, no. 5834, pp. 83–86, Jul. 2007, doi: 10.1126/science.1143254.

[11] K. Hwang, J. Cho, D. Kim, J. Park, J. Kwon, S. Kwak, H. Park, and S. Ahn, "An autonomous coil alignment system for the dynamic wireless charging of electric vehicles to minimize lateral misalignment," *Energies*, vol. 10, no. 3, p. 315, Mar. 2017, doi: 10.3390/en10030315.

[12] R. Tavakoli and Z. Pantic, "Analysis, design, and demonstration of a 25-kW dynamic wireless charging system for roadway electric vehicles," *IEEE J. Emerg. Sel. Topics Power Electron.*, vol. 6, no. 3, pp. 1378–1393, Sep. 2018, doi: 10.1109/jestpe.2017.2761763.

[13] M. J. Chabalko and A. P. Sample, "Three-Dimensional charging via multimode resonant cavity enabled wireless power transfer," *IEEE Trans. Power Electron.*, vol. 30, no. 11, pp. 6163–6173, Nov. 2015, doi: 10.1109/tpel.2015.2440914.

[14] W. M. Ng, C. Zhang, D. Lin, and S. Y. Ron Hui, "Two-and three-dimensional omnidirectional wireless power transfer," *IEEE Trans. Power Electron.*, vol. 29, no. 9, pp. 4470–4474, Sep. 2014, doi: 10.1109/tpel.2014.2300866.

[15] D. Lin, C. Zhang, and S. Y. R. Hui, "Mathematic analysis of omnidirectional wireless power transfer—Part-II three-dimensional systems," *IEEE Trans. Power Electron.*, vol. 32, no. 1, pp. 613–624, Jan. 2017, doi: 10.1109/TPEL.2016.2523506.

[16] D. Lin, C. Zhang, and S. Y. R. Hui, "Mathematical analysis of omnidirectional wireless power transfer—Part-I: Two-dimensional systems," in *IEEE Trans. Power Electron.*, vol. 32, no. 1, pp. 625–633, Jan. 2017, doi: 10.1109/TPEL.2016.2523500.

[17] C. Zhang, D. Lin, and S. Y. R. Hui, "Ball-joint wireless power transfer systems," *IEEE Trans. Power Electron.*, vol. 33, no. 1, pp. 65–72, Jan. 2018, doi: 10.1109/tpel.2017.2700898.

[18] J. Kim and J. Jeong, "Range-adaptive wireless power transfer using multiloop and tunable matching techniques," *IEEE Trans. Ind. Electron.*, vol. 62, no. 10, pp. 6233–6241, Oct. 2015, doi: 10.1109/tie.2015.2420041.

[19] S. Assawaworrarit, X. Yu, and S. Fan, "Robust wireless power transfer using a nonlinear parity–time-symmetric circuit," *Nature*, vol. 546, pp. 387–390, Jun. 2017, doi: 10.1038/nature22404.

[20] J. Schindler, A. Li, M. C. Zheng, F. M. Ellis, and T. Kottos, "Experimental study of active LRC circuits with $\mathcal{PT}$ symmetries," *Phys. Rev. A, Gen. Phys.*, vol. 84, no. 4, Oct. 2011, Art. no. 040101, doi: 10.1103/PhysRevA.84.040101.

[21] J. Schindler, Z. Lin, and J. M. Lee, "$\mathcal{PT}$-symmetric electronics," *J. Phys. A, Math. Theor.*, vol. 45, no. 44, 2012, Art. no. 444029, doi: 10.1088/1751-8113/45/44/444029.

[22] A. U. Hassan, H. Hodaei, M.-A. Miri, M. Khajavikhan, and D. N. Christodoulides, "Nonlinear reversal of the $\mathcal{PT}$-symmetric phase transition in a system of coupled semiconductor microring resonators," *Phys. Rev. A, Gen. Phys.*, vol. 92, no. 6, Dec. 2015, Art. no. 063807, doi: 10.1103/PhysRevA.92.063807.

[23] J. Zhou, B. Zhang, W. Xiao, D. Qiu, and Y. Chen, "Nonlinear parity-time-symmetric model for constant efficiency wireless power transfer: Application to a drone-in-flight wireless charging platform," *IEEE Trans. Ind. Electron.*, vol. 66, no. 5, pp. 4097–4107, May 2019, doi: 10.1109/tie.2018.2864515.

[24] Z. Karantalov, *Inductance Calculation Manual*. Beijing, China: Mechanical Industry Press, 1992.

[25] J. Lammeraner and M. Stafl, *Eddy Currents*. London, U.K.: Iliffe Books,1966.

[26] F. Liu, Y. Yang, D. Jiang, X. Ruan, and X. Chen, "Modeling and optimization of magnetically coupled resonant wireless power transfer system with varying spatial scales," *IEEE Trans. Power Electron.*, vol. 32, no. 4, pp. 3240–3250, Apr. 2017, doi: 10.1109/tpel.2016.2581840.

[27] A. Namadmalan, "Self-oscillating pulse width modulation for inductive power transfer systems," *IEEE J. Emerg. Sel. Topics Power Electron.*, to be published, doi: 10.1109/jestpe.2019.2916425.

ZHENG ZHANG was born in Changde, China, in 1995. He received the B.S. degree in building electrical and intelligent from Xiangtan University, Xiangtan, China, in 2017. He is currently pursuing the M.S. degree in power electronics and power drives with the South China University of Technology, Guangzhou, China.

His main research direction is wireless power transfer systems and its application.

BO ZHANG (Senior Member, IEEE) was born in Shanghai, China, in 1962. He received the B.Sc. degree in electrical engineering from Zhejiang University, Hangzhou, China, in 1982, the M.S. degree in power electronics from Southwest Jiaotong University, Chengdu, China, in 1988, and the Ph.D. degree in power electronics from the Nanjing University of Aeronautics and Astronautics, Nanjing, China, in 1994.

He is currently a Professor with the School of Electric Power, South China University of Technology, Guangzhou, China. He has authored or coauthored over 450 articles and holds 102 patents. He has authored eight monographs. His research interests include wireless power transfer technology and nonlinear analysis and control of power supplies.